

## The Squall Line Thunderstorm: Numerical Experimentation

CARL E. HANE<sup>1,2</sup>

*Dept. of Meteorology, Florida State University, Tallahassee 32306*

(Manuscript received 24 October 1972, in revised form 30 July 1973)

### ABSTRACT

The structure and mechanism for maintenance of the Great Plains squall line thunderstorm are studied through formulation of a two-dimensional, time-dependent numerical model. The environmental conditions known to be favorable for squall line development and maintenance include a convectively unstable air mass whose motion is characterized by strong vertical shear of the horizontal wind. These conditions are used to specify an environment in an  $x$ - $z$  plane upon which a disturbance is superimposed. The appropriate physical equations are integrated forward in time to study changes in the motion, thermal and moisture fields in and around the squall line thunderstorm.

The vertical shear of the horizontal environmental wind is varied from one experiment to another with the result that broader and longer lasting cloud circulations occur in the stronger shear cases. Specific areas where three-dimensional effects must be important are discussed from an examination of variable fields during periods when the system undergoes a lessening in intensity. It is found that the system, rather than reaching a quasi-steady state, undergoes a series of developments (three or four during a 100-min period) as measured by the time variation of maximum updraft speed, downdraft speed, and rainwater mixing ratio. However, the system structure during the intense stage of each development is basically the same as that during the other developments, and strongly resembles the structure envisaged in qualitative physical models suggested in the past: 1) the updraft and downdraft exist side by side, the updraft possessing an upshear tilt from the vertical through the lower half of the troposphere; 2) rain produced in the updraft falls into the downdraft, strengthening or maintaining the downdraft due to its own weight and through negative buoyancy produced by evaporation; and 3) maintenance of the downdraft results in a strongly convergent region in lower levels downshear from the system and a tendency toward updraft maintenance or redevelopment. The implication is that the squall line thunderstorm, once initiated, maintains itself by interaction with its synoptic environment as long as it remains within an environment containing convectively unstable air whose motion is characterized by moderate-to-strong vertical shear.

### 1. Introduction

It has long been recognized that the type of thunderstorm which comprises the squall line of the Great Plains differs in several important ways from the "air mass" thunderstorm which commonly occurs in the southeastern United States in summer. The two types differ in several important respects aside from the differences in location relative to synoptic-scale disturbances and differences in the severity of the accompanying weather. Two differences are particularly noteworthy:

1) The squall line type is more persistent in the sense that individual thunderstorms either last longer or create the conditions necessary for their redevelopment following dissipation. The air mass thunderstorm is more short-lived except in cases where it is under the influence of such effects as the sea breeze or orography.

2) The environmental conditions differ in the two cases. Strong vertical shear of the horizontal wind and dryness of the air in mid-tropospheric levels are characteristics of the squall line thunderstorm environment, whereas lesser shear and considerable moisture at all levels are usually the case in the air mass thunderstorm environment.

More than 20 years ago, Newton (1950) suggested certain reasons why squall lines tend to occur in an environment whose horizontal motion is characterized by moderate-to-strong vertical shear. He reasoned that the largest convective clouds, by means of their strong updrafts and downdrafts, tend to distribute in-cloud horizontal momentum rather uniformly through the vertical. The resulting patterns of convergence and divergence in such a case favor downshear propagation of the squall line. Newton also mentioned the importance of strong vertical shear in the intensification of the downdraft. In the low levels, there is relative inflow of warm moist air on the downshear side and, because of the strong vertical shear, there is relative inflow in middle levels on the upshear side. This dry middle-level

<sup>1</sup> A portion of this study was carried out while affiliated with the National Center for Atmospheric Research, which is sponsored by the National Science Foundation.

<sup>2</sup> Present affiliation: Atmospheric Sciences Department, Pacific Northwest Laboratories, Batelle Memorial Institute, Richland, Wash.

air overtaking the system is very effective in the evaporation of falling rain and in the production of negative buoyancy on the upshear side where the downdraft is located. Intensification of the downdraft leads to more low-level convergence ahead of the system and to the tendency toward new updraft development.

Another important point which has been discussed frequently is that regarding the shape of the updraft within the mature cloud. Some evidence from RHI radar displays suggests an upshear tilt of the updraft. Bates (1961), Browning and Ludlam (1962) and Newton (1963) have all stated that it is likely that the main updraft in large storms is inclined in an upshear direction through an appreciable depth of the cloud. Fig. 1 is a schematic drawing which combines and summarizes this idea and the earlier idea concerning the strong shear. Here, the two-dimensional air flow within a traveling convective storm is shown with the downdraft within the cloud coexisting just upshear from the upshear tilting updraft. Such an arrangement of updraft and downdraft allows the rain to fall from the updraft, relieving the updraft of this retarding force, and allows the rain to fall into a region which is most favorable for the production of negative buoyancy through evaporation. Because of the strong shear, the updraft is continually replenished by the incoming, warm, moist low-level air and the downdraft continually sustained by the dry middle-level air overtaking the system. Thus, the system is able to convert the potential energy of its environment into the kinetic energy which is necessary for its maintenance, an idea first stated by Normand (1946).

The above-mentioned ideas can only be verified or rejected by analyses of direct or indirect observations taken in actual squall line situations. The temporal and spatial separation of these observations must be such as to resolve the air properties within the large cumulonimbi which comprise the squall line. No such observations now exist; any mesoscale networks of surface and radiosonde stations which now operate (or have operated) are not (or were not) designed for resolving scales within even large clouds, but more for the purpose of studying the immediate environment of these clouds. In-cloud behavior can only be inferred from these observations. It seems reasonable, therefore, to turn to numerical modeling of these systems, using the environmental data which now exist as a guide in specifying initial and boundary conditions.

Formulation of such a numerical model necessarily depends upon previous work in the area of numerical simulation of convective clouds in both one and two dimensions. The two-dimensional area of study was initiated by Malkus and Witt (1959) in a study of dry convection. Moisture was introduced a few years later by Ogura (1963). The work of Kessler *et al.* (1961–64) in the area of microphysics of cloud and rain led to the inclusion of liquid water in these models in the late 1960's and early 1970's by Árnason *et al.* (1968), Orville

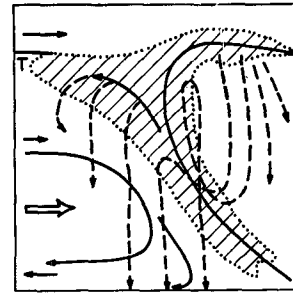


FIG. 1. Schematic representation of the motion field within a middle-latitude cumulonimbus in wind shear (relative winds far away from storm indicated on left). Condensation is shown in hatched region, and some paths of precipitation particles are indicated (dashed lines). Motion field (relative) is indicated by long solid arrows (after Ludlam, 1961).

and Liu (1969), Murray (1970) and Takeda (1971). Srivastava (1967) had earlier included explicit treatment of cloud and rain in a one-dimensional experiment. Other one-dimensional experiments, including those of Squires and Turner (1962), Simpson and Wiggert (1969), Weinstein (1970), Ogura and Takahashi (1971), and Danielsen *et al.* (1972), have included consideration of the ice phase in their calculations.

Attempts in the past aimed specifically at numerically modeling the squall line have been very few. Early attempts by Sasaki (1959) and also by Ogura and Charney (1962) did not explicitly treat the individual clouds and their internal circulations, but dealt with the problem on a much larger scale. More recently, Takeda has modeled what he calls a "long lasting" cloud, but this is a smaller cloud than the squall line thunderstorm and occurs within an environment wind field unlike that which is consistently observed in squall line situations. Schlesinger (1972) has modeled deep moist convection in shear using a coarse horizontal grid with the result that the intensity of convection increases with increasing low-level moisture supply and decreases with increasing mid-tropospheric wind shear.

It is clear that quantitative calculations are needed to test the validity of the basic ideas in the qualitative squall line thunderstorm models. Advances in the numerical modeling of moist convection in recent years appear to have elevated knowledge and research techniques in this area to the level where they might be applied fruitfully to the squall line problem. The remainder of this paper will be concerned with just such an application.

## 2. The model

Ideally, in modeling the squall line, one would like to include time dependence and all three space dimensions, but current computer capacity does not permit this. There is good reason to believe that, in the case of the squall line, variations along the line might be neglected in the study of some of the basic aspects. The squall line is always much longer than it is wide, so that

at least near its center it might be considered quasi-two-dimensional (especially near the ground where the cold downdrafts from individual cells merge to form a nearly continuous temperature drop line). In addition, the ideas of those who have looked at and analyzed the observations and who have formulated physical models have been expressed mainly in terms of two-dimensional processes. The consequences of imposing this two-dimensional restriction will be discussed in the result section.

To initiate the calculations, a disturbance is superimposed upon an environment possessing the characteristics noted in the Introduction, and the appropriate physical equations are integrated numerically to study the time evolution of the system. It is the goal here that the model simulate the observed long-lasting character of the squall line through either (i) the attainment of a quasi-steady cooperative updraft-downdraft system continuously interacting with its environment, or (ii) a succession of developments, each containing the ingredients necessary for redevelopment following dissipation. In addition, the effect of vertical shear of the environmental wind will be studied by variation of the shear from one experiment to another.

Certain physical processes and environmental characteristics known to be essential in the squall line and which are included in the model are listed below. Following this, other processes and characteristics will be listed which are not included.

1. The environment includes convectively unstable air whose motion is characterized by strong vertical shear (variable from one experiment to another).
2. Condensation and evaporation processes and their associated temperature changes are included.
3. Liquid water is included "in bulk," assuming a Marshall-Palmer (1948) distribution of drop sizes. The fall of precipitation-sized liquid water is taken into account.
4. Turbulent mixing by scales of motion not resolvable by the 400 m grid are parameterized in terms of known grid-scale variables.

Processes and characteristics which are considered less essential and are not included are as follows:

1. Horizontal changes in quantities in the direction of squall line elongation are neglected.
2. The solid state of water is not included.
3. Horizontal and temporal changes in air density are not taken into account, except implicitly in the buoyancy term of the vorticity equation.
4. Radiational effects are neglected.
5. Surface effects are neglected, including surface evaporation and frictional effects to the extent that they are not taken into account implicitly in the boundary conditions.

The basic model equations include time-dependent equations for the vorticity, temperature, and for the

mixing ratios of water vapor, cloudwater and rainwater. The other basic equation relates the vorticity to the streamfunction. The vorticity equation may be shown (Hane, 1972) to be

$$\begin{aligned} \frac{\partial \eta}{\partial t} = & -u \frac{\partial \eta}{\partial x} - w \frac{\partial \eta}{\partial z} - \eta D_v - \frac{g}{T_v} \frac{\partial T_v}{\partial x} + g \frac{\partial}{\partial x} (q_l + q_c) \\ & + c_M \left\{ \frac{\partial}{\partial z} \left[ \frac{\partial w}{\partial x} (u'' - u) \right] - \frac{\partial}{\partial x} \left[ \frac{\partial w}{\partial x} (w'' - w) \right] \right\} \\ & + \frac{\partial}{\partial x} \left( \nu_x \frac{\partial \eta}{\partial x} \right) + \frac{\partial}{\partial z} \left( \nu_z \frac{\partial \eta}{\partial z} \right), \quad (2.1) \end{aligned}$$

where the vorticity  $\eta = \partial u / \partial z - \partial w / \partial x$ ,  $u$  is the horizontal wind speed,  $w$  the vertical wind speed,  $D_v = \partial u / \partial x + \partial w / \partial z$ ,  $T_v$  is the virtual temperature,  $q_l$  the rainwater mixing ratio,  $q_c$  the cloudwater mixing ratio,  $c_M$  the turbulent mixing coefficient,  $u''$  and  $w''$  are the time-invariant vertical distributions of the horizontal and vertical motion, respectively, characteristic of the environment, and  $\nu_x$  and  $\nu_z$  the time-space dependent horizontal and vertical eddy viscosity coefficients.

The viscosity coefficients are determined from the local flow characteristics, i.e.,

$$\begin{aligned} \nu_x &= c_1 \nu_z, \\ \nu_z &= c_2 (\Delta z)^3 \left[ c_1 \left( \frac{\partial \eta}{\partial x} \right)^2 + \left( \frac{\partial \eta}{\partial z} \right)^2 \right], \end{aligned}$$

where in this study  $\Delta z = 400$  m,  $c_1 = 1$  and  $c_2 = 0.91$ . This formulation is to some extent based upon the work of Leith (1968). It has been summarized by O'Brien (1971), and has been applied in a numerical problem by Hane (1970). The coefficients ( $\nu_x = \nu_z$ ) in these experiments vary over a wide range—typically  $10^{-1}$  to  $2.5 \times 10^3$ . The equation of continuity takes the form

$$\frac{\partial}{\partial x} (\rho u) + \frac{\partial}{\partial z} (\rho w) = 0, \quad (2.2)$$

where  $\rho$  is air density. A streamfunction may thus be defined

$$\rho u = \frac{\partial \psi}{\partial z} \quad \text{and} \quad \rho w = -\frac{\partial \psi}{\partial x},$$

leading to the diagnostic relation between vorticity and streamfunction:

$$\nabla^2 \psi - \frac{1}{\rho} \frac{\partial \psi}{\partial z} \frac{\partial \rho}{\partial z} = \rho \eta. \quad (2.3)$$

A term containing the horizontal gradient in air density has been neglected here. The first law of thermo-

dynamics has the form

$$\frac{\partial T}{\partial t} = -u \frac{\partial T}{\partial x} - w \left( \frac{\partial T}{\partial z} + \Gamma_d \right) + \frac{1}{c_p} \frac{dQ}{dt} + c_M \left| \frac{\partial w}{\partial x} \right| (T'' - T) + \nu_\theta \nabla^2 T, \quad (2.4)$$

where  $T$  is the absolute temperature,  $\Gamma_d$  the dry adiabatic lapse rate,  $(1/c_p)(dQ/dt)$  the latent heating or cooling rate,  $T''$  the time-invariant vertical profile of temperature characteristic of the environment, and  $\nu_\theta$  the constant ( $500 \text{ m}^2 \text{ sec}^{-1}$ ) coefficient of thermal eddy diffusion. The equations involving the moisture are three in number:

$$\frac{\partial q_v}{\partial t} = -u \frac{\partial q_v}{\partial x} - w \frac{\partial q_v}{\partial z} + c_M \left| \frac{\partial w}{\partial x} \right| (q_v'' - q) + \nu_\theta \nabla^2 q_v + \text{evaporation} - \text{condensation} \quad (2.5)$$

$$\frac{\partial q_c}{\partial t} = -u \frac{\partial q_c}{\partial x} - w \frac{\partial q_c}{\partial z} + c_M \left| \frac{\partial w}{\partial x} \right| (q_c'' - q_c) + \nu_\theta \nabla^2 q_c - \text{autoconversion} - \text{accretion} - \text{evaporation} + \text{condensation} \quad (2.6)$$

$$\frac{\partial q_l}{\partial t} = -u \frac{\partial q_l}{\partial x} - w \frac{\partial q_l}{\partial z} + \frac{\partial}{\partial z} (q_l V_T) + \frac{q_l V_T}{\rho} \frac{\partial \rho}{\partial z} + \text{autoconversion} + \text{accretion} - \text{evaporation}. \quad (2.7)$$

Here,  $q_v$  is the water vapor mixing ratio and  $q_v''$  and  $q_c''$  are time-invariant vertical profiles of the water vapor and cloudwater mixing ratios, respectively, characteristic of the environment. The turbulent mixing term, appearing in all the time-dependent equations except Eq. (2.7), is discussed at length in the Appendix. The autoconversion, accretion and rainfall velocity expressions (included within the next five equations) follow from the work of Kessler *et al.* (1961-64):

$$\left. \frac{\partial q_l}{\partial t} \right)_{\text{auto}} = K_a (q_c - q_{cr}),$$

where  $q_{cr}$  is a critical cloudwater content below which no autoconversion occurs (in this study  $K_a = 10^{-3} \text{ sec}^{-1}$  and  $q_{cr} = 0.05 \text{ gm kg}^{-1}$ );

$$\left. \frac{\partial q_l}{\partial t} \right)_{\text{accretion}} = 1.5 \times 10^3 \pi N_0 \rho \Gamma(3.5) q_c / (4\lambda^{3.5}),$$

where  $N_0 = 10^7 \text{ m}^{-4}$ ,  $\rho$  is air density,  $\Gamma$  is the gamma function symbol defined by

$$\Gamma(n) = \int_0^\infty e^{-x} x^{n-1} dx,$$

and  $\lambda$  is defined by

$$\lambda = \left[ \frac{\pi \rho_w N_0}{q_l} \right]^{1/2},$$

where  $\rho_w$  is the density of liquid water; and the "effective terminal velocity" ( $\text{cm sec}^{-1}$ ) of the rainwater distribution which is found in Eq. (2.7) is calculated by

$$V_T = 1.5 \times 10^3 \Gamma(4.5) / [\lambda^{1/2} \Gamma(4)].$$

The condensation process in upward-moving saturated air is accomplished through a "dynamic adjustment" followed by a "static adjustment" as described by Murray and Anderson (1965). Evaporation of cloudwater takes place instantaneously whenever cloudwater exists in unsaturated air. If rainwater is present in cloudless unsaturated air, it is evaporated at a rate determined by

$$\left. \frac{\Delta q_v}{\Delta t} \right)_{\text{evap}} = C_e N_0^{-1/8} (q_s - q_v) (\rho q_l)^{13/20},$$

where  $C_e = 7.72 \times 10^{-6} \text{ m}^{3.35} \text{ gm}^{0.35} \text{ sec}^{-1}$  and  $q_s$  is the saturation mixing ratio of the air.

### 3. Computational procedures, boundary conditions, and initial conditions

The time-integration procedures used is a predictor-corrector scheme, which means that Eqs. (2.1), (2.3), (2.4), (2.5), (2.6) and (2.7) are solved twice during each time step. The length of each time step is variable, depending upon the magnitude of air motions, but generally lies in the 15-20 sec range. The grid distance is 400 m in both the horizontal and vertical, while the total domain of integration varies in size from 25.6 to 38.0 km (horizontally) by a constant 12.8 km (vertically).

A 9-point scheme, the Arakawa Jacobian (Arakawa, 1966), is used for the evaluation of advective terms, while centered space differences are used in general elsewhere. Eq. (2.3) is solved by successive over-relaxation in cases where a faster scheme cannot be used. In cases where the number of grid points,  $N$ , in each direction satisfies the condition that  $N = 2^n + 1$  ( $n = 1, 2, 3, \dots$ ), a faster technique formulated by Buneman (1969) is employed.

No flow is allowed through the top and bottom boundaries. The flow through the lateral boundaries is time invariant, changes in the interior flow not being allowed to affect the motion through the lateral boundaries. Other variables along the lateral boundaries are determined by an inflow-outflow condition at those boundaries; if the flow is inward, the boundary values are held constant, and if the flow is outward, a quasi-Lagrangian technique outlined by Shapiro and O'Brien (1970), is used. Temperature and water vapor are determined along the lower boundary by setting the

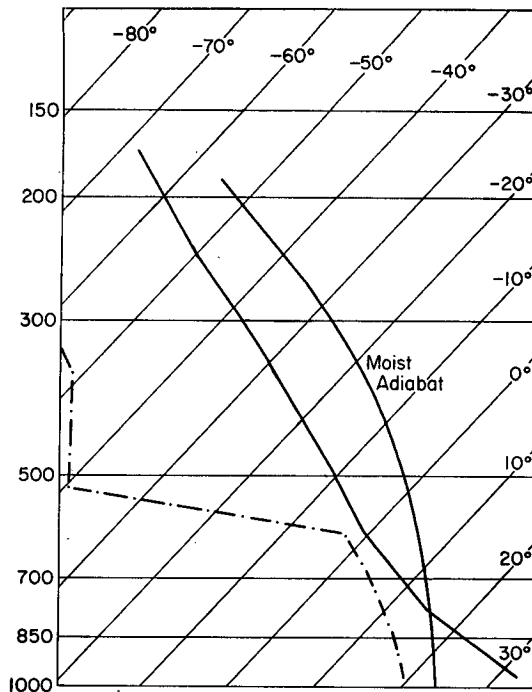


FIG. 2. Initial vertical distribution of environmental temperature (solid line) and environmental dew point (dash-dotted line).

anomaly of temperature and of water vapor equal to that at the next higher row of grid points (400 m).

As was mentioned previously, the purpose here is to study the structure and tendency for self-maintenance of the squall line thunderstorm. The problem of squall line development is another question and is not considered here. With this in mind, the form and intensity of the initial perturbation is not important, as long as it does not influence the structure of the system at later times. Various initial perturbations were tried with the result that there was a tendency toward convergence upon a common solution after an amount of time which increased as a function of the initial difference between perturbations. In the cases reported upon here, the initial perturbation is a well-developed thunderstorm-like circulation. Other cases have been tried beginning with a "dry line" type situation, where a low-level convergent zone is superimposed upon a low-level horizontal moisture gradient. In the latter case the same basic structure is arrived at after 2-3 hr as was arrived at after a few minutes in the former case. This being the case, only the initial environmental profiles and not the initial perturbation will be shown here.

Fig. 2 shows the environmental temperature and moisture profiles which were used in all the experiments. The environment is quite unstable with a sharp drop in the moisture profile between 600 and 500 mb. The sounding is typical of observed soundings taken prior to squall line passage. Moist adiabatic ascent of air parcels from cloud base would in this case produce warm anomalies of 12-13C if no mixing were to occur. Fig. 3

shows the profiles of the environmental wind used in each experiment. The curves plotted show wind speeds relative to the earth, although the winds used in the computations are those relative to the moving disturbance. The numbers in parentheses next to each curve denote the approximate rate of motion ( $\text{m sec}^{-1}$ ) of the system in each case. In practice, each of these speeds is determined by finding that speed which, when subtracted from the air motion relative to the earth, renders the disturbance stationary with respect to the side boundaries throughout the period of the disturbance's existence. Since there is net upward motion in the domain, with convergence in low levels and divergence aloft, the wind profile to the left of the storm is different from that on the right. The profiles shown in Fig. 3 are the mean of the left and right profiles. Fig. 4 compares the profile in the strongest shear case with the profile in a well-documented storm over England (see Browning and Ludlam, 1962) and that for a weakening squall line of moderate intensity which passed over the National Severe Storms Laboratory mesonet network in Oklahoma in May of 1968. Although the rawinsonde ascents were terminated at 400 mb in the Oklahoma case, the strong shear in the lowest 3 km can be seen in each case. The shear in middle levels in the model experiment lies in an intermediate range relative to the two observed cases.

#### 4. Results of computations

Table 1 summarizes the experiments which were run using the various environmental wind profiles. Two of the experiments (R6 and R7) were run on a larger grid

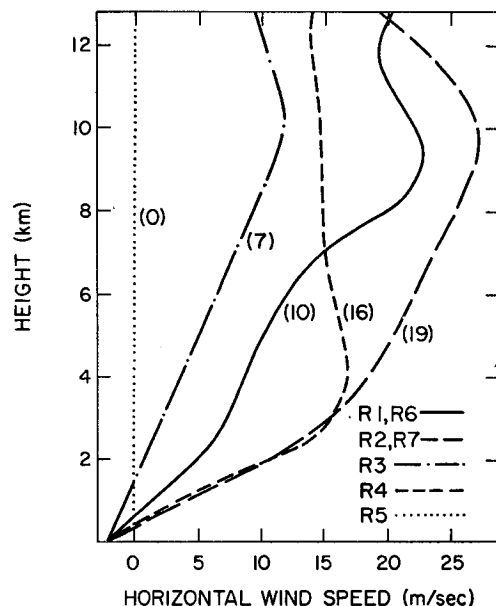


FIG. 3. The vertical distribution of the horizontal environmental wind used in the model experiments. Numbers in parentheses denote the approximate rate of motion ( $\text{m sec}^{-1}$ ) of the system. See Table 1 for identification of experiments.

for a longer period of time using the same shear distributions as were used in shorter experiments (R1 and R2, respectively).

The results of Experiment R1 after about 5 min of integration will be described in some detail here in order that various features in the results to be presented at other times will be better understood. Fig. 5 shows the results of R1 at 5.6 min and includes the two-dimensional fields of streamfunction, rainwater mixing ratio, temperature anomaly and vertical motion. The rainwater distribution and the cloudwater outline are superimposed upon the streamfunction field in the top section of this figure and in each of the other cases that will be shown. The motion field at this time shows the coexistence of updraft and downdraft; the updraft exhibits an upshear tilt and the downdraft originates in middle levels located for the most part beneath the updraft. There is relative inflow from the left-hand side at middle levels, a portion of which enters into the downdraft circulation. The downdraft, upon reaching the ground, spreads both forward and to the rear. The cloud outline shows a tilted structure also, with new development of cloud occurring on the lower right (downshear) side. The outline of the cloud on the left side follows the line of no vertical motion between the updraft and the downdraft. The upper portion of the cloud is spreading in the horizontal, mainly in the downshear direction. The rainwater pattern shows an increasing accumulation of liquid water along the left hand edge of the updraft (maximum value  $> 7 \text{ gm kg}^{-1}$ ). This location is favored because of production of rainwater from cloudwater in the updraft and a combination of advection by the tilted updraft with the fall of raindrops relative to the air which contains them. Rainwater reaches the ground at this time, but not in great amounts.

The temperature anomaly pattern (deviation from initial environmental profile) at this time shows a warm region with a maximum slightly greater than  $7\text{C}$  located along the axis of the updraft, due to condensational heating in the updraft. A relatively cool area exists just to the left of the warm area, extending upward from a cold region at the ground (anomaly  $> -6\text{C}$ ). This relatively cool region results from evaporation of rain

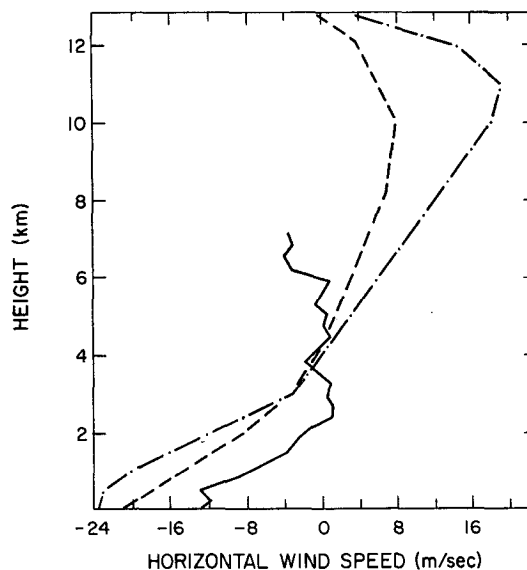


FIG. 4. Comparison of vertical shear of horizontal wind relative to moving storm in one of the model experiments with that in two observed situations. Dashed: horizontal wind used in model Experiment R2 (strong shear); dash-dotted: Wokingham storm (see Browning and Ludlam, 1962); solid: squall line of 29 May 1968 over Oklahoma mesonetwork.

in the downdraft. To the left of this a warm region (maximum anomaly  $> 3\text{C}$ ) exists, resulting from dry adiabatic warming in descending air with little or no rain in it. To the right of the updraft is a slightly cool region resulting from dry adiabatic cooling in upward moving air containing little or no condensate.

The vertical motion pattern shows the maximum upward motion to be more than  $22 \text{ m sec}^{-1}$  at a height of about 7 km. The downward motion is slightly greater than  $10 \text{ m sec}^{-1}$  at about 3 km. There are regions of downward "compensation" outside the cloud, located on the right in the upper troposphere and on the left, merging with the rain-augmented downdraft, between the cloud and the left boundary.

The equivalent potential temperature distribution is shown in Fig. 6 for this same time. The pattern reveals that very dry air is being brought downward by the downdraft from the middle-level environment. The downdraft is unsaturated for the most part, the influx of dry air and downward motion being so great that the evaporation of rain does not maintain saturation. The equivalent potential temperature is not uniformly constant in the updraft as it would be if the motion were completely moist adiabatic, but the effects of mixing are seen to result in a decrease in equivalent potential temperature with height even along the updraft core.

The results of Experiment R1 are shown at 16.3 min in Fig. 7. The most apparent change here is the lessened intensity and lack of organization in the system. At least three reasons may be given for this change in shape

TABLE 1. Summary of the model experiments.

Number	Title	System speed (m sec <sup>-1</sup> )	Number of grid points
R1	moderate shear	10	65×33
R2	strong shear	19	65×33
R3	weak shear	7	65×33
R4	mixed shear	16	65×33
R5	no shear	0	65×33
R6	moderate shear	10	96×33
R7	strong shear	19	96×33

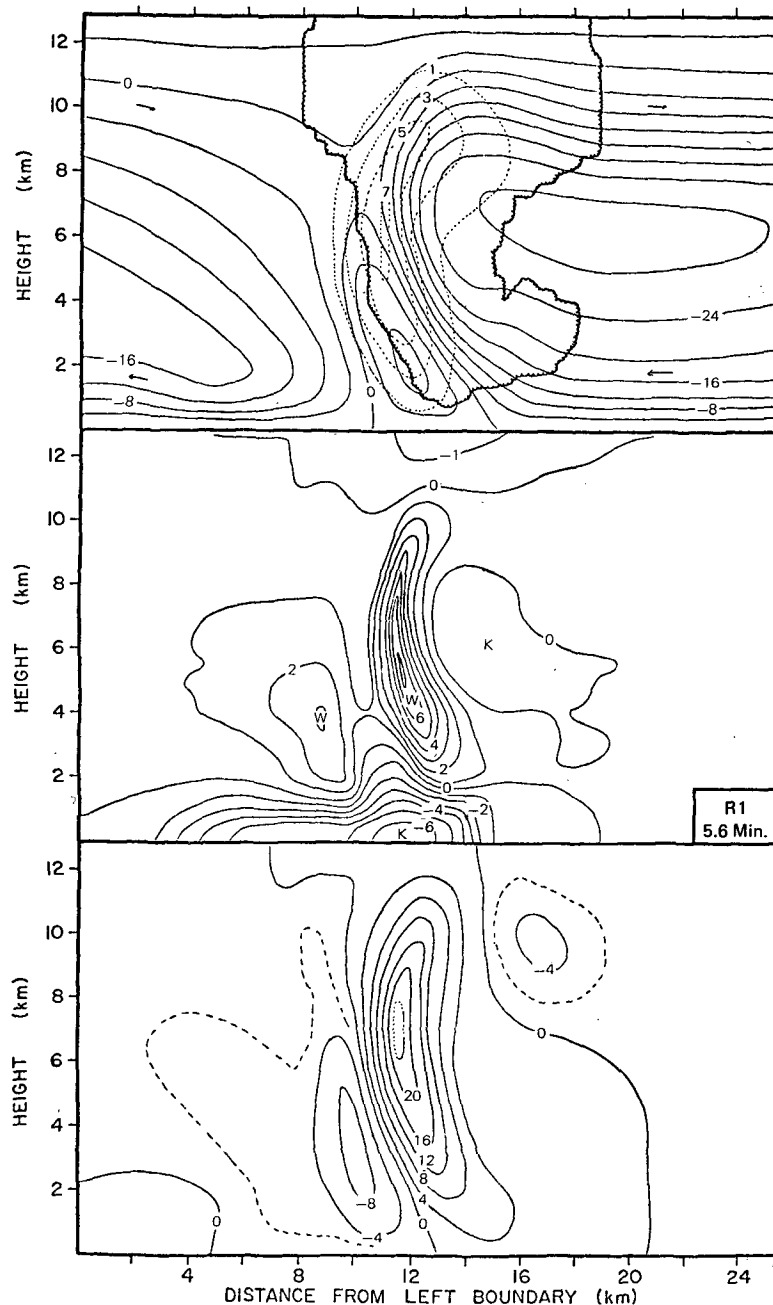


FIG. 5. Variable fields for Experiment R1 at 5.6 min. Upper: solid lines are streamfunction ( $10^3 \text{ kg m}^{-1} \text{ sec}^{-1}$ ); dashed lines rainwater mixing ratio ( $\text{gm kg}^{-1}$ ); scalloped lines cloudwater mixing ratio outline; middle: temperature anomaly ( $^{\circ}\text{K}$ ); lower: vertical wind speed ( $\text{m sec}^{-1}$ ).

and intensity, and all are related to the two-dimensional constraint imposed in this model.

1) The air in the downdraft upon reaching the ground must spread either forward or to the rear, whereas in nature it can and does spread to some extent into the third dimension. Since the updraft originates at the micro-cold front at the leading edge of this cold downdraft air, the lower updraft undergoes an excessive

downshear displacement. This means that in order for the updraft to maintain itself at its original intensity, it must regenerate in middle levels on its right-hand side. This regeneration is prevented because:

2) The downward motion in middle levels to the right of the original cloud is advecting dry air into the updraft. This downward motion is more intense than it would be in nature where some of the "compensation" takes place out of the plane of this model.

3) The strong relative left-to-right flow in upper levels must take part in the in-cloud circulation in this two-dimensional case, whereas in nature a great deal of the air must go around the cloud, since the precipitation-filled cloud must to some extent act as an obstacle to the flow. Thus, the strong horizontal winds aloft in this two-dimensional case tend to bend the updraft in a downshear sense in upper levels, and some rain tends to fall on the right-hand side of the cloud. This creates additional difficulty for the regeneration process to occur continuously in that vicinity.

The results shown in Fig. 7 show some of these features quite clearly. The cold air at the ground with more than 8C negative anomaly has spread considerably downshear from the updraft location at middle levels. The vertical motion pattern shows two distinct upward maxima with strong downward motion directly above the low-level maximum. The strong left-to-right flow is seen to bend the upper part of the cloud in a downshear direction.

The results of Experiments R1 and R6 agree well during the period of integration common to both. The results of Experiment R6 at 28.9 min are shown in Fig. 8. At this time little remains of the original cloud; however, a new cloud is growing at the leading edge of the cold air near the surface. The situation, then, at this time is essentially one where the ambient flow is simply ascending over the cold pool near the ground and the flow in the upper half of the troposphere is undisturbed.

The results are next shown at 41.9 min (Fig. 9) when a very significant redevelopment has taken place. The cloud and cloud circulation are here comparable to those shown at 5.6 min (Fig. 5). The basic structure in both cases is the same: the updraft is tilted upshear in lower levels and downshear in upper levels, and the rain is falling from the updraft into the downdraft. The maximum amount of rain ( $>7 \text{ gm kg}^{-1}$ ), maximum temperature anomaly ( $>6\text{C}$ ), and maximum upward motion ( $>20 \text{ m sec}^{-1}$ ) are comparable to those in the first development. Differences result from (i) the influence of the initial state in the first development in combination with (ii) the effects of the two-dimensionality mentioned previously. These differences include the higher penetration of the cloud in the first development, the extensive anvil in the second development, and the differences in tilt of the axis of maximum upward motion. The cloud in the initial state extended to the top boundary, so that the first development included cloud extending to the upper boundary. The second development takes place through an area which, minutes earlier, was unsaturated so that penetration to the top boundary is much more difficult. The anvil in the second development includes the remains of previous developments, whereas in the first development any anvil which was produced had to have been produced as a result of that development only. The fact that the

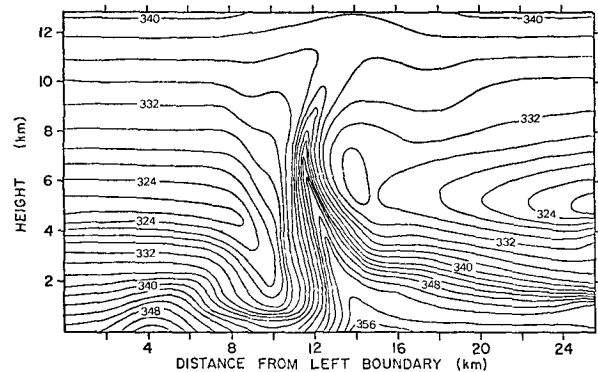
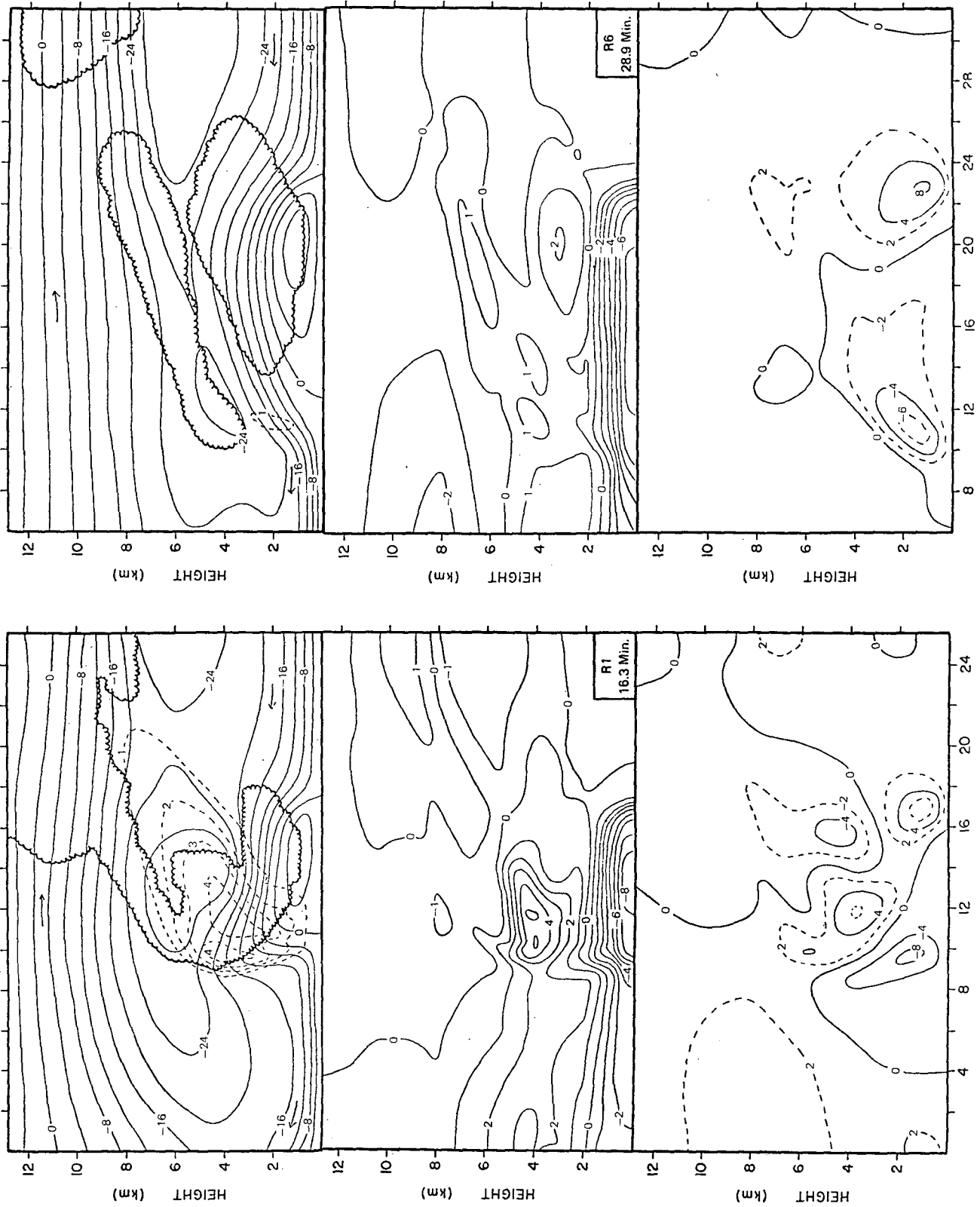


FIG. 6. The equivalent potential temperature ( $^{\circ}\text{K}$ ) distribution for Experiment R1 at 5.6 min.

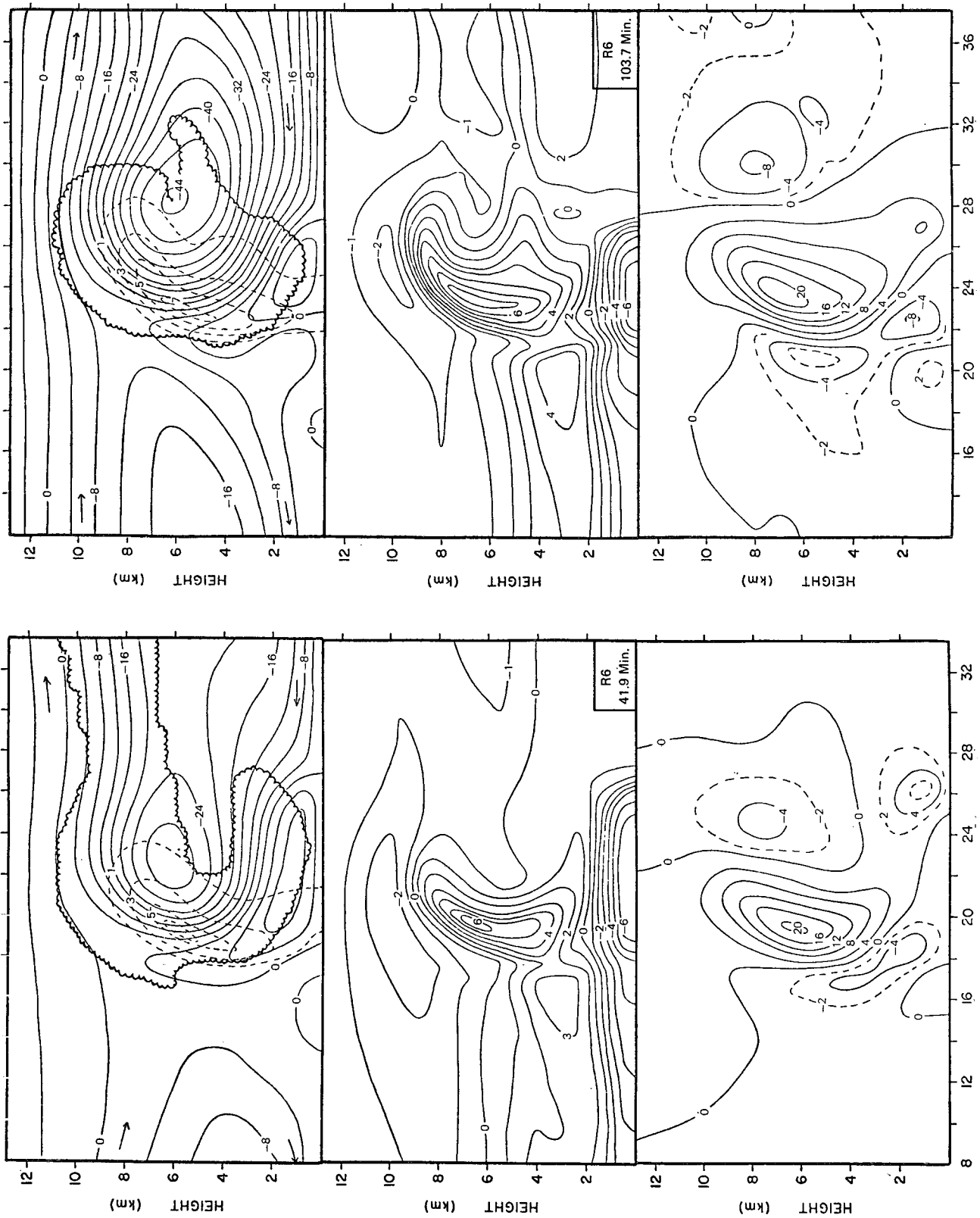
initial state included a tilted updraft led to a tilted updraft to higher levels in the first development. In the second development the adverse two-dimensional effect of strong winds aloft leads to a shift from upshear tilt to downshear tilt at a lower level. Also, the extensive spreading of the cold air at the ground in the second development has led to an extreme upshear tilt of the updraft at lower levels, until at the time shown in Fig. 9 there is an actual separation in the maxima in the updraft.

The second development clearly verifies the assertion that the form of the initial state does not predetermine the result. For instance, the fields shown in Fig. 8 might have been used as an initial state, and yet the basic structures and intensities shown in Figs. 5 and 9 are the same, although differing in detail. Fig. 10 summarizes the time evolution of the disturbance for the entire period of integration in Experiment R6. The maxima of various disturbance features are here plotted versus time with no designation of the location of the maxima. It should be noted that the location of the maximum upward motion varies with time, but in a fairly continuous manner. Discontinuous jumps in location occur only when one development loses intensity and another begins. This is also true of the downward motion maximum and rainwater maximum. Fig. 10 shows that there are actually four significant developments (including the first) during this  $\sim 100$ -min period. Each development includes a cloud and circulation pattern with the same basic structure as shown in Figs. 5 and 9. Each development follows the same cycle with respect to the evolution of maximum updraft speed, maximum downdraft speed, and maximum rainwater mixing ratio.

Referring again to Fig. 10, in the case of each development the maximum upward motion is followed by a maximum in rainwater mixing ratio and then by a maximum in downdraft speed. The interpretation here is that rain continues to be produced in the updraft even though the speed is decreasing. At the same time the rain is falling, and it does so at a greater rate (rela-



FIGS. 7 (left) and 8 (right). As in Fig. 5 except for R1 at 16.3 min and R6 at 28.9 min. Abscissa is distance (km) from left boundary.



Figs. 9 (left) and 11 (right). As in Fig. 5 except for R6 at 41.9 min and R6 at 103.7 min. Abscissa is distance (km) from left boundary.

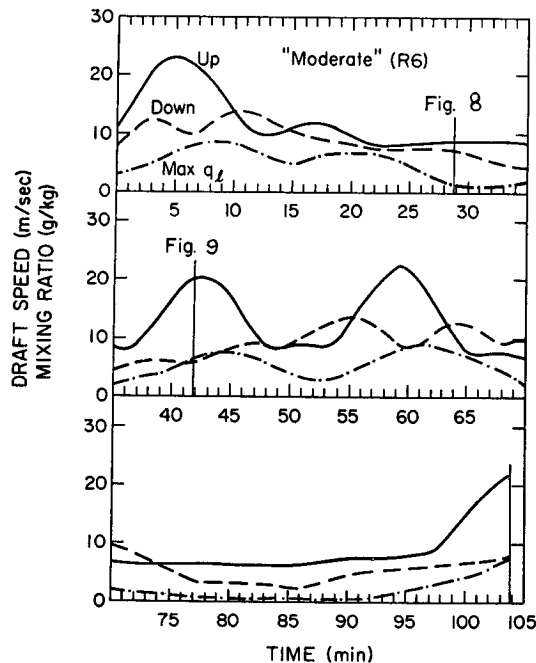


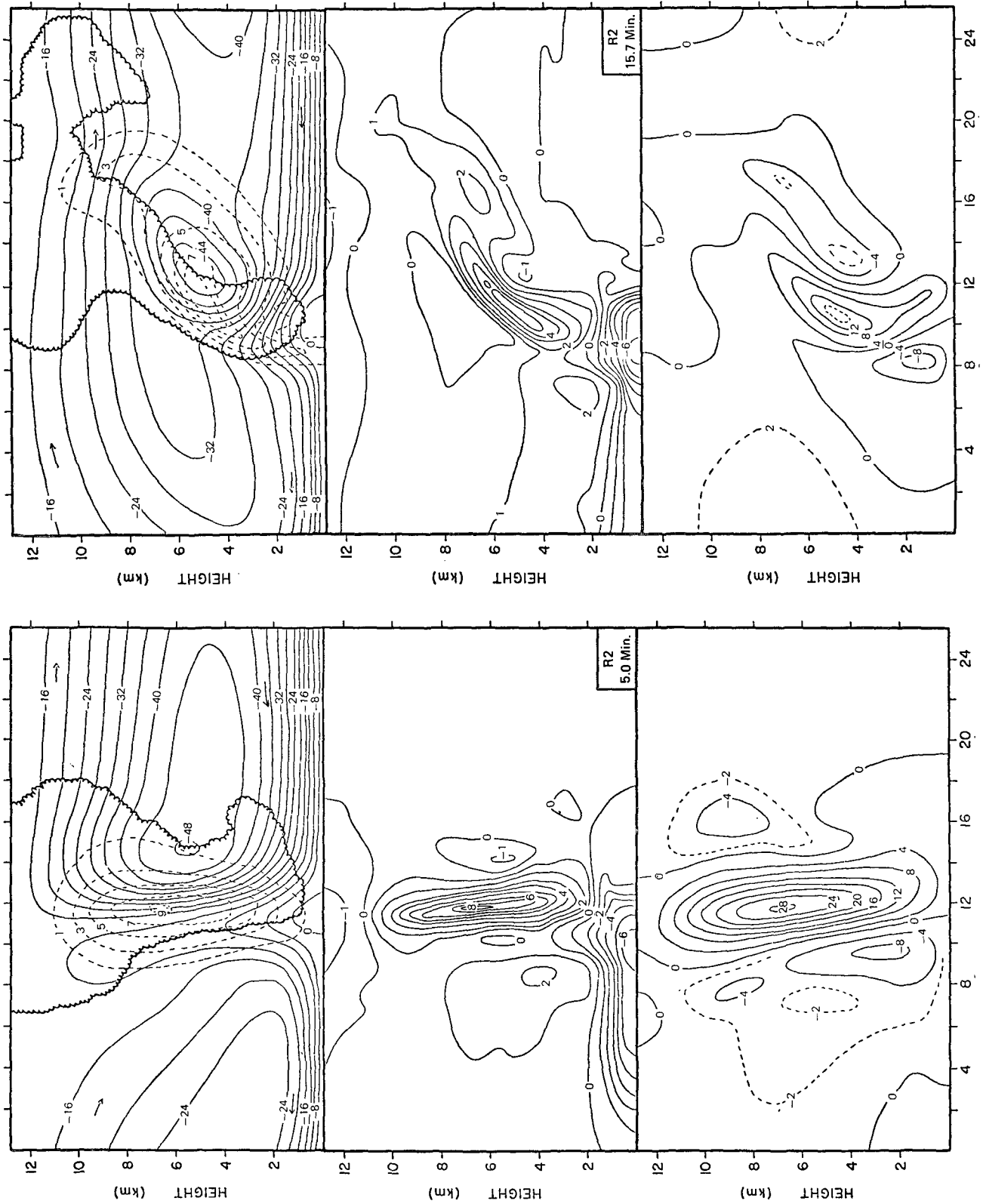
FIG. 10. For Experiment R6, the variation with time of the magnitude of the maximum upward motion (solid), maximum downward motion (dashed), and maximum rainwater mixing ratio (dash-dotted).

tive to the earth) as the updraft speed decreases. The two effects (production and falling) result in a maximum in rainwater mixing ratio which lags the maximum upward motion by about 2 min in each case. As the rain falls, the downdraft speed increases due to negative buoyancy resulting from evaporational cooling and due to the weight of the rain. Thus, the maximum downdraft speed lags the maximum rainwater mixing ratio by about 3 min and the maximum updraft speed by about 5 min in each case. It should also be noted that there are actually two maxima in the downdraft speed (temporal maxima) during each development. First, the increase in maximum updraft speed and vertical development of the updraft is accompanied by an increase in maximum downdraft speed purely through mass compensation. This downward compensation decreases in maximum value as it spreads over a larger area during the time that the updraft is at its maximum intensity. This is followed by the concentration of this downward motion over a smaller area and an increase in maximum value as rain produced in the updraft falls on the upshear side of the cloud.

An explanation is also called for as to why the developments occur when they do and why there are sometimes long quiet periods between developments. A close examination of the temperature field during the entire period of the integration reveals that the one stable feature is the pool or "dome" of cold air near the ground. Associated with this at all times is a region of upward motion (with a maximum of 6–9 m sec<sup>-1</sup>) and

cloud near the leading edge of the cold air at a height of about 1.5 km. Whether this upward motion leads to deep convection appears to depend upon the sign of the vertical motion in mid-tropospheric levels directly above the upward maximum in low levels. Downward motion in middle levels above this upward maximum during the time of strong developments results either from downward compensation for upward motion in the cloud or from rain falling to the right of the cloud because of the downshear tilt in middle to upper levels. Both of these reasons given for downward motion in this area are seen to result from the aforementioned adverse effects of the two-dimensionality. Therefore, in the absence of these effects a greater tendency toward a quasi-steady-state updraft would probably be achieved. Instead, in this two-dimensional case the convection occurs in pulses or spurts with strong updrafts being rather short-lived. In long periods where no developments occur, such as 70–95 min in Experiment R6 (Fig. 10), another explanation must be sought. The two developments at 43 and 59 min combine to produce a great deal of rain and a great deal of downward motion (Fig. 10). Although conditions are favorable at about 65–70 minutes for another development, it does not occur. The reason for this is that a short time later the right-hand edge of this large area of downward motion spreads until it is actually directly over the low-level upward motion which is constantly produced by the cold dome. It is not until about 85 min that this downward motion has weakened sufficiently to allow the beginnings of a new development. This is signaled in Fig. 10 by a slow increase in the maximum downward motion beginning at 86–87 min and associated with an upward spread of the area of upward motion. It is not until about 97 min that the maximum upward motion rises above that constant value which is ever present at the edge of the cold dome. The growth is slow to this point because the air in middle levels has become dry due to downward motion. The final development is shown in Fig. 11. It is seen that the basic structure of the cloud circulation is the same as in the previous developments shown. The areal extent of the cloud at this time is not large since it is growing into relatively dry air.

The results of Experiments R3, R4 and R5 will not be shown here; however, a brief description of each will now be given. In the weak-shear experiment (R3), a loss of intensity and organization occurs rather quickly in that the upward motion area is narrower because of the weaker relative low-level inflow. Also separation of the updraft occurs more dramatically than in the moderate-shear case because of the more rapid left-to-right movement of the surface cold air relative to the mid-level updraft. Experiment R4, where the wind shear is very strong in the lowest 3 km and very weak and of the opposite sign above that level, was run in an attempt to see the effect of not having strong winds in upper levels, which in a two-dimensional experiment,



Figs. 12 (left) and 13 (right). As in Fig. 5 except for R2 at 5.0 min and R2 at 15.7 min. Abscissa is distance (km) from left boundary.

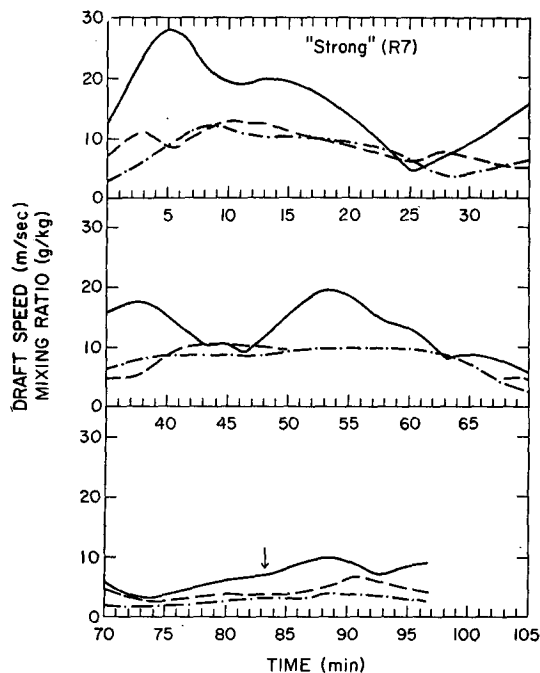


FIG. 14. As in Fig. 10 except for Experiment R7. The arrow denotes the time when the maximum upward motion shifts to near the boundary.

have an exaggerated effect upon the upper parts of convective clouds. The result was that the upshear tilting updraft had a longer lifetime than in other experiments, and that the downdraft was considerably stronger because the rain had fallen in the same area for a long time. Experiment R5 was run with no environmental wind shear. This development most closely resembles the latter two-thirds of the life cycle of an air mass cumulonimbus, as described by Byers and Braham (1949). The motion is primarily upward in a non-tilting updraft in the early stages with a large accumulation of liquid water, followed by the development of a strong downdraft and the dissipation of the updraft as the rain falls out.

Experiment R2 differs from R1 in that the vertical shear of the horizontal wind is stronger in the mean than in R1, and much stronger below 3 km (see Fig. 3). The results of Experiment R2 at about 5 min are shown in Fig. 12. The updraft shows a slight upshear tilt, but not so pronounced as in R1 (cf. Fig. 5). More rain is present ( $>9 \text{ gm kg}^{-1}$ ) than in Experiment R1 at this time because of the stronger ( $>28 \text{ m sec}^{-1}$ ) and broader updraft and additional condensation. This rain, because of the more vertical updraft, remains suspended in the updraft to a greater extent than in R1 and as a result does not maintain so strong a downdraft during much of its early history. Once again, downward "compensation" is fairly strong ( $>4 \text{ m sec}^{-1}$ ) to the right of the updraft in upper levels in the anvil outflow.

Fig. 13 shows the results of Experiment R2 at 15.7 min. Strong downward motion has developed to the

right of the cloud in middle levels due to the large amount of rain falling there. The cloud remains an entity as does the warm air within it, but both show a pronounced downshear tilt. The maximum amount of rainwater at this time remains near the  $9 \text{ gm kg}^{-1}$  value. Comparison of this figure with Fig. 7 reveals both common and diverse features in the results at this time. In the strong-shear case the cloud circulation remains more organized in spite of the high horizontal winds in upper levels tending to bend the top downshear. There are two apparent reasons for this degree of organization: 1) The area of upward motion is stronger and broader in the strong-shear case so that the erosion by the incorporation of strong environmental winds is less rapid than in the moderate-shear case. 2) There is no separation in the lower updraft as in Fig. 7 because the relative inflow in low levels is much stronger in the strong-shear case and does not allow a forward movement of the cold air produced in the downdraft.

Fig. 14 shows the time evolution of Experiment R7 (R2). The maximum upward motion obtained early in Experiment R7 was  $28.3 \text{ m sec}^{-1}$  compared to  $23.3 \text{ m sec}^{-1}$  in Experiment R6. It is also clear from this figure that there is a greater tendency for a long-lasting cloud in this case. It is seen here that once again, following the loss of organization and intensity of the first development, redevelopment occurs, and more than once. In this case two developments occur following the first with maximum upward motion at about 38 and 53 min. An additional development would occur toward the end, but strong upward motion along the right boundary results in cloud growth there and the flow of potentially warm air to the fourth development is cut off.

It is seen that the timing of the developments in this experiment is approximately the same as in Experiment R6. In comparing Experiments R6 and R7 where the only difference is in the environmental wind shear, the arrival at clear-cut conclusions as to the effect of wind shear is hampered by the adverse effect of the combination of two-dimensionality and strong shear. Although the secondary developments in Experiment R7 are less intense in terms of maximum upward motion than the first (and slightly less intense than the redevelopments in Experiment R6), the clouds in Experiment R7 are somewhat broader and longer lasting. The lessened upward motion maxima in R7 result from the severe tilting in middle and upper levels by the strong shear, and the broadness and longevity are probably due to the increased relative inflow of potentially warm air in low levels. Several other points may be emphasized here in examining Fig. 14. Maximum downdraft speeds at their peak times are generally less and maximum rainwater amounts greater than in the moderate-shear case (R6). Because the strong shear tends to tilt the upper half of the updraft downshear, the rain falls less into the downdraft and tends to accumulate in the updraft. At the same time the downdraft strength does not reach the values that it does in

Experiment R6 because the area beneath the upshear tilted updraft (restricted to the lowest levels) is so small. These points are well illustrated by reference to Fig. 12, even though the effect of strong shear in this case in tilting the updraft downshear is compensated for to some extent by the upshear tilt imposed in the initial state. Reference once again to Fig. 14 reveals that in this period between maxima in the updraft speed, there is virtually no decrease in maximum rainwater mixing ratio. In fact, during a period of almost 35 min the maximum rainwater mixing ratio does not drop below  $5 \text{ gm kg}^{-1}$ . Thus, if such a storm were viewed by PPI radar, the impression would be gained that a single development of long duration were occurring, whereas there are actually two maxima in the upward motion. Viewed by RHI radar, however, a depression in the height of echo return would possibly be discernible at a time between updraft maxima.

Several calculations were made in order to verify that certain of the model results fall within the range of values observed in natural situations. These included rainfall rate, rainfall amount, distribution of temperature in the cold dome, and radar reflectivity. The calculated maximum rainfall rate (instantaneous) was slightly more than 10 inches  $\text{hr}^{-1}$  and occurred in the strong-shear case at about 53 min, resulting from the second strong development which occurred at about 37 min. In the case of each development in both the moderate- and strong-shear experiments, the maximum rainfall at the ground follows the maximum updraft speed by 15–20 min. Rainfall rates are considerably higher in the strong-shear case compared to the moderate-shear case, consistent with the generally larger values of rainwater mixing ratio in the strong-shear case. However, total rainfall accumulations at a fixed point on the ground, taking into account the system speeds, are in the range 0.3–0.4 inch in both the strong- and moderate-shear experiments since the speed of the system is greater in the strong-shear case. It is also worthwhile noting that maximum horizontal wind speeds behind the micro-cold front are in the 45–50 kt range. These should be compared with sustained winds in nature rather than short-lived gusts which cannot be resolved with 400 m resolution.

The next comparison involved the temperature distribution within the cold "dome." The maximum temperature drop at the lower boundary resulting from the passage of the squall front is in general 7–10C. This compares favorably with observations. The vertical extent of the cold dome is in general about 2 km (to 770 mb) in the model calculations. For comparison of the vertical structure with observations a vertical line 16 km from the left boundary is chosen in Experiment R6 at 28.9 min (Fig. 8). The difference between the calculated temperature at each height along this line and the initial environmental temperature at each height is plotted in Fig. 15. Also plotted for comparison is an equivalent quantity for an observed case. Sound-

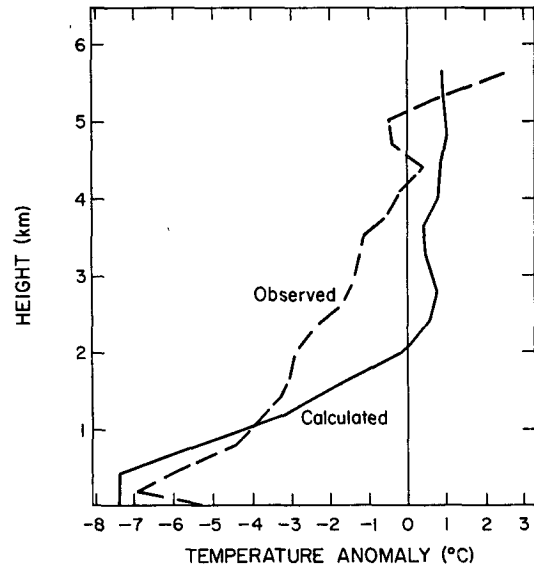


FIG. 15. Temperature anomaly within the cold dome for Experiment R6 at 28.9 min (solid line) and for an observed case of 29 May 1968 (dashed lines).

ings are considered at four stations spaced about 16 mi apart in the Oklahoma meso network. A squall line passed all four stations at approximately the same time (2130 CST) on 29 May 1968. Soundings were taken at approximately 2100 and 2200 CST (before and after squall line passage). The temperature change between the two soundings was computed at each station at 300-m height intervals, with the average of the four station profiles also being shown in Fig. 15. It should be noted here that neither of these curves represents conditions within the downdraft, but rather conditions within the cold dome which exists as a result of the convection. The magnitude of the temperature drop in the model calculations agrees well with the observed between the surface and about 1.5 km, but the observed case shows a greater total decrease in temperature (2–3C colder) between 2 and 3 km. The depth of the cold dome is therefore greater in the observed case, extending upward to about 550 to 600 mb. The warmer temperatures above 1.5 km in the model calculations probably result from the moderate downward motion and adiabatic warming in middle-level dry air to the left of the cloud and rain area. This downward motion may not be so strong at this location in nature. Differences might also result from particular conditions in the observed case which was chosen.

Some basis for comparison is also needed in order to insure that the calculated rainwater mixing ratios within the cloud are within the range of those which might be found in nature. No direct measurements within large convective storms have been made, but indirect measurements exist in the form of radar reflectivity data. The reflectivity factor  $Z$  is defined to be  $\sum_i n_i D_i^6$ , where  $D_i$  is the diameter of the  $i$ th drop

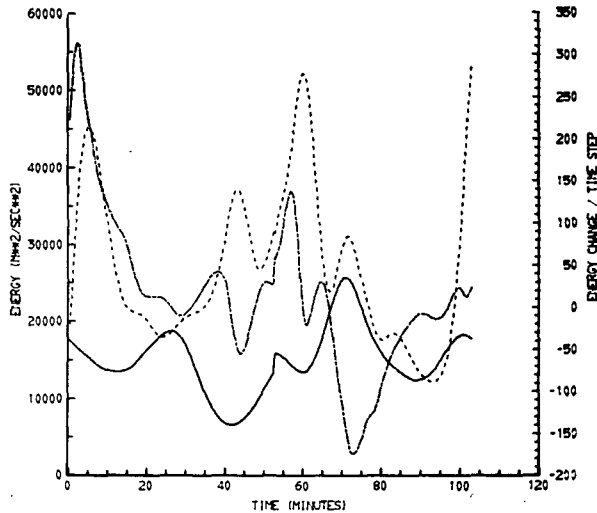


FIG. 16. Time variation of the integrated mean kinetic energy (solid), eddy kinetic energy (dashed), and energy transformation per time step by the eddy motions in shear (chained).

size and  $n_i$  is the number of drops at that diameter per cubic meter. The echo intensity is often expressed in terms of the quantity  $10 \log_{10} Z$  where  $Z$  is in units of  $\text{mm}^6 \text{m}^{-3}$ . Measurements of this quantity taken in the Wokingham storm indicate a maximum value of 71 (considering the entire time of observation of the storm) while at most times the maximum value was near 65. In the model experiments maximum rainwater mixing ratios during periods of significant developments range from about 7 to  $11.8 \text{ gm kg}^{-1}$ . Taking into account the Marshall-Palmer raindrop distribution, one can calculate the quantity  $10 \log_{10} Z$  for the model calculations also. This quantity is computed to be 61.5 for a mixing ratio of  $10 \text{ gm kg}^{-1}$  and 56.3 for  $5 \text{ gm kg}^{-1}$ . It should be noted that the presence of hail (either wet or dry) must have increased  $10 \log_{10} Z$  in the case of the Wokingham storm.

Besides the high reflectivity values, other radar features have often been noted in squall line or severe thunderstorm situations. These features include (i) the echo "wall," formed by the leading edge of the precipitation near the ground; (ii) the "forward overhang," occupying a region to the right of the main updraft; and (iii) the "echo-free vault," where the strong updraft enters the cloud between the wall and forward overhang. These features are observed in the model results in the shape of the rainwater mixing ratio pattern in certain instances. The best examples are not shown, but to some extent these features can be seen in Fig. 13 (upper). There, the rainwater pattern in upper levels is somewhat distorted by the effect of strong shear. The updraft is probably sufficiently strong to produce an echo-free region, but because the rainwater is treated in bulk rather than taking into account discrete drop sizes, the shape of the pattern is smoothed compared to features observed by radar.

## 5. Energy calculations

The time evolution of the convection arrived at here is characterized by an aperiodic series of developments rather than by a quasi-steady state. The question of how the squall line thunderstorm maintains itself in the presence of moderate or strong shear, becomes in this case a question of how the convective activity is able to repeatedly develop in the presence of strong shear. This is an entirely different question from that of the manner in which the initial development occurs. In the model case there is always strong low-level convergence at the leading edge of the cold air, whereas in the case of the initial development in nature, there is no such dome of cold air. As was mentioned earlier, it is not the purpose of this research to study the initial development process, but to gain a better understanding of the maintenance mechanism.

In order to examine the convective developments from a different approach, additional calculations were made and will now be briefly described. Energy equations were formulated from the vorticity and temperature equations of the model in a manner similar to that of Asai (1964). The flow was divided into mean and eddy parts, and equations for the area-integrated mean kinetic, eddy kinetic, mean potential, and eddy potential energies were formulated.

The time variations of mean and eddy kinetic energies are shown in Fig. 16. The peaks in eddy kinetic energy coincide closely with the peaks in maximum vertical velocity (see Fig. 10), since most of the eddy kinetic energy is contained in the convective circulations. A large part of the increase in eddy kinetic energy accompanying each development is a result of a conver-

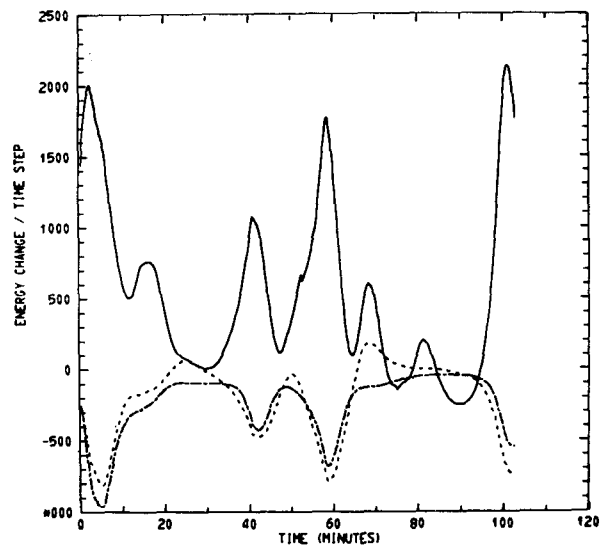


FIG. 17. Time variation of the integrated change in eddy kinetic energy per time step by transformation from eddy potential energy by buoyant accelerations (solid), weight of liquid water (dashed), and turbulent mixing between cloud and environment (chained).

sion from eddy potential energy through buoyant accelerations. This contribution and those due to the falling of liquid water and turbulent mixing processes are shown in Fig. 17. The latter two processes are maximized during periods of development when they contribute toward a decrease in the eddy kinetic energy. Also significant is a conversion from mean kinetic to eddy kinetic energy by the tilted updrafts and downdrafts in the shear flow. This term has the form

$$\frac{\partial}{\partial t} \iint K_e dA = - \iint \frac{1}{2} u' w' \frac{\partial \bar{n}}{\partial z} dA,$$

where  $K_e$  is the eddy kinetic energy, and  $u'$  and  $w'$  the eddy components of the horizontal and vertical velocity, respectively. The time variation of this term (Fig. 16) reveals that maximum values occur during periods when the eddy kinetic energy is increasing (when convective circulations are developing). The magnitude of this term is small compared to other terms when integrated over the entire area; however, in the convective region of tilted updrafts and downdrafts, it is very likely equal in magnitude to other terms. In the lower updraft region it contributes to a large positive change in  $K_e$ , whereas in the upper updraft region it contributes oppositely, so that the integrated value is small. Thus, the upshear-tilted updraft in the shear flow contributes to the development of the convection by a conversion of mean kinetic to eddy kinetic energy. This analysis, however, is not an adequate means of answering the question of how the tilted updraft structure comes about in the first place.

As was implied in the discussion of the results, it is felt that the upshear tilt of the updraft in the lower troposphere results from the tendency toward conservation of horizontal momentum in the updraft. The air in the lowest levels has a strong right-to-left momentum relative to the storm, and as it rises in the updraft it retains some of this, resulting in a tilt of the updraft toward the left (upshear) with height. The presence of the cold dome is most essential here, since it forces air upward from the lowest levels, which provides for the maximum difference in horizontal momentum between the updraft and environment to be attained.

Reference was made in the Introduction to the conversion of environmental potential energy to the kinetic energy of the storm circulation. One should more properly term this environmental energy as latent energy, since it is the capacity of the dry middle-level air to evaporate rain and to be cooled and the capacity of the moist low-level air to condense and to be warmed, which ultimately drive the storm circulation. The vertical shear of the environmental wind allows for the incorporation of this dry middle-level air and moist low-level air from opposite sides of the convective circulation, so that the conversion process is most efficient. The storm not only continually incorporates fresh air from the environment, but also incorporates it

in such a way that the updraft and downdraft do not interfere with one another.

## 6. Conclusions

One goal of this research which was stated in the Introduction was to test the validity of the basic ideas put forth in the qualitative physical models. The basic structure of the in-cloud circulations arrived at in this model agrees quite well with the basic structure hypothesized in these models. The means for maintenance or redevelopment is the same in both cases, although the numerical results indicate a less steady convective system than the qualitative models. In both cases the updraft-downdraft combination interacts with the environment in such a way that either maintenance or redevelopment is favored.

The effects of vertical shear in the environmental wind distribution are masked to some extent because of the fact that strong shear in a two-dimensional case tends to bend the top of the cloud downshear, leading to its dissipation. However, it appears from the results of all the experiments that strong shear leads to more intense, longer lasting, and broader cloud circulations compared to cases with moderate or weak shear. The reason for this is simply that the strongly-sheared systems translate at higher speeds and consequently the relative inflow of warm moist low-level air is stronger. Another way of saying this is that the divergence field produced by the convective circulation itself is stronger in the stronger shear case. The vertical distribution of environmental moisture also enters strongly here, but this parameter was not varied in these experiments. Also important in a few cases in nature is the net divergence in the region immediately surrounding the squall line. However, in most cases it is observed that the region of localized upward motion in which the squall line develops does not move in phase with the line itself. The divergence field producing upward motion surrounding the line is only important to the *full lifetime* of the line in those few cases where both are stationary or moving at the same speed.

The results of the calculations point to three specific areas where the third dimension is important in the squall line thunderstorm circulation. These areas are: (i) the region where the downdraft encounters the solid earth, (ii) the regions outside the cloud where downward motion is taking place to "compensate" for upward motion in the updraft, and (iii) the upper half of the cloud where the environmental flow relative to the cloud is strong. In connection with (ii) Murray (1970) ran two numerical models of tropical cumulus convection, one rectangular and the other cylindrical. The maximum downward velocity outside the cloud was  $\sim 15\%$  of the maximum in-cloud upward velocity in the cylindrical model, but  $\sim 40\%$  in the rectangular model. The region mentioned under (iii) becomes more important in strong-shear situations where a large percentage of the

flow must pass around the edges of the cloud in order that it exist. Observational evidence (Fankhauser, 1971) strongly suggests that in the case of *isolated* cumulonimbi at least a partial obstacle effect is present near the 500-mb level (part of the air flowing around, and part into the upshear side of the cloud). In the case of the squall line, this effect might be slightly less important, since the environmental flow would at times encounter a nearly solid line of towers in middle and upper levels and the air would be forced to take part in the in-cloud circulations to a greater extent.

The most important conclusion obtained here is that, based upon quantitative calculations in a two-dimensional model, the squall line thunderstorm, once initiated, is self-maintaining, deriving its kinetic energy from the potential (latent) energy of its environment. It is also inferred from these results that continued maintenance or subsequent redevelopments depend solely upon the tendency of the squall line to remain within an environment possessing the proper thermodynamic and kinematic structure.

*Acknowledgments.* I am most grateful to Prof. N. E. LaSeur for his numerous suggestions during the course of this research, to Dr. C. W. Newton for his comments upon the work, and to Prof. T. N. Krishnamurti and Prof. J. J. O'Brien for their individual help with certain computational aspects of the problem in the early stages. The work was supported by Grants E22-64-68(G) and E22-19-71(G) from the National Severe Storms Laboratory, Norman, Okla. The computing was done at the Florida State University Computing Center under Grant GJ-367 from the National Science Foundation, and at the Computing Facility of the National Center for Atmospheric Research, which is sponsored by the National Science Foundation.

APPENDIX

The Turbulent Mixing Terms

Here the rate of mass exchange between updraft (or downdraft) and environment due to small-scale eddy motions is considered, and an expression for the mixing term to be used in the model equations is found. Let  $\dot{M}$  be the flux of mass through the bottom of the area surrounding a grid point located at level  $z$  (Fig. 18). In going from the level  $z - \Delta z/2$  to  $z + \Delta z/2$  (where  $\Delta z$  is the vertical grid interval) it is assumed that there occurs a flux of mass  $\Delta \dot{M}$  inward and an equal flux of

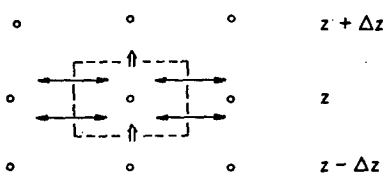


FIG. 18. Schematic representation of the turbulent mixing occurring within a sample grid area.

mass  $\Delta \dot{M}$  outward due to sub-grid-scale eddy motions. Let the quantity  $q$  represent some property of the air (such as temperature) at the grid point in question and let  $q''$  represent the value of that variable at some horizontal distance in the environment. Let the amount of change in  $q$  due to mixing be denoted  $\Delta q$ . It must be true that the flux of  $q$  through the top of the area is equal to the flux through the bottom less what leaves through the sides plus what enters through the sides, i.e.,

$$(q + \Delta q)\dot{M} = q\dot{M} - q\Delta \dot{M} + q''\Delta \dot{M},$$

so that

$$\Delta q = (q'' - q) \frac{\Delta \dot{M}}{\dot{M}},$$

or

$$\left. \frac{\Delta q}{\Delta t} \right]_{\text{mixing}} = (q'' - q) \frac{1}{M} \frac{\Delta \dot{M}}{\Delta t}.$$

It now remains to arrive at a reasonable value for the quantity  $(1/M) (\Delta \dot{M}/\Delta t)$ .

Laboratory experiments with buoyant jets and plumes, as noted by Squires and Turner (1962), have provided estimates for the entrainment constant  $\alpha$  in the following equation based upon mass continuity for a plume which is adding mass at each level at a rate proportional to the local upward velocity and to the surface area:

$$\frac{1}{M} \frac{\Delta \dot{M}}{\Delta t} = \frac{w}{M} \frac{\Delta \dot{M}}{\Delta z} = \frac{2\alpha w}{R},$$

where  $w$  is the vertical velocity of the air within the plume,  $R$  the radius, and  $\alpha$  the entrainment constant. This sort of relation applied to a *top-hat* profile of vertical velocity, i.e., one which is constant at all radii and drops discontinuously to zero at the edge of the plume or jet. The values found experimentally for  $\alpha$  have all been in the neighborhood of 0.1.

In the case of a thunderstorm updraft, the horizontal variation of the vertical velocity is probably much smoother than that in the laboratory plumes and jets. The following assumption is made for the mixing rate in the thunderstorm updraft (or downdraft):

$$\frac{1}{M} \frac{\Delta \dot{M}}{\Delta t} = c_M \left| \frac{\partial w}{\partial x} \right|.$$

This expression may be considered a logical extension of the expression which is used in the one-dimensional plume and jet models, since in the two-dimensional case here the quantity  $\partial w/\partial x$  replaces the  $w/R$  of the one-dimensional case. The mixing rate here is thus proportional to the horizontal shear of the upward motion rather than to the updraft speed itself. Thus, the effects of mixing are minimized along the core of the updraft and maximized along the edges of the updraft

where the shear is large (where eddy motions should be most vigorous). The constant  $c_M$  must be determined in such a way that it is consistent with the above-mentioned laboratory measurements to the extent that this is possible.

It is here assumed that the rate of change of some quantity  $q$  due to mixing, integrated over the entire width of the updraft, is the same for (a) a top-hat profile updraft and (b) an equivalent updraft with a smoothly-varying profile. In (b) the updraft profile is such that its average vertical velocity is equal to the constant top-hat velocity and that the average deviation of  $q$  from its environmental value (which is denoted here  $\delta = q'' - q$ ) is the same as the constant deviation in the top-hat profile. For simplicity, it is assumed that (b) has a sinusoidal profile for  $w$  and for  $\delta$  (Fig. 19), i.e.,

$$\left. \begin{aligned} w &= \frac{w_M}{2} \left[ 1 + \sin \pi \left( \frac{x}{R} + \frac{1}{2} \right) \right] \\ \delta &= \frac{\delta_M}{2} \left[ 1 + \sin \pi \left( \frac{x}{R} + \frac{1}{2} \right) \right] \end{aligned} \right\}$$

The maximum values for  $w$  and  $\delta$  are here denoted by  $w_M$  and  $\delta_M$ . Therefore, the average values of  $w$  and  $\delta$  are  $w_M/2$  and  $\delta_M/2$  and these are the values which are used here in the specification of the top-hat profiles.

The local time-rate-of-change of the quantity  $q$  due to mixing is

$$\left. \frac{\partial q}{\partial t} \right|_{\text{mix}} = (q'' - q) \frac{1}{M} \frac{\Delta M}{\Delta t} = \delta \frac{1}{M} \frac{\Delta M}{\Delta t}$$

This expression will now be integrated over the half-width of the updraft (since it is symmetric) for both the top-hat (TH) and the sinusoidal (S) profiles. The integrated rate of change in the case of the top-hat profile is found to be

$$\begin{aligned} I_{\text{TH}} &\equiv \int_0^R \left. \frac{\partial q}{\partial t} \right|_{\text{TH}} dx = \int_0^R \delta \frac{1}{M} \frac{\Delta M}{\Delta t} dx = \int_0^R \frac{2\alpha}{R} \delta w dx \\ &= \int_0^R \frac{\delta_M}{2} \frac{w_M}{2} \left( \frac{2\alpha}{R} \right) dx = \frac{\delta_M w_M \alpha}{2} \end{aligned}$$

For the sinusoidal profile

$$\left| \frac{\partial w}{\partial x} \right| = \left| \frac{w_M \pi}{2R} \left[ \cos \pi \left( \frac{x}{R} + \frac{1}{2} \right) \right] \right|$$

Noting that in the range 0 to  $R$

$$\left| \cos \pi \left( \frac{x}{R} + \frac{1}{2} \right) \right| = -\cos \pi \left( \frac{x}{R} + \frac{1}{2} \right),$$

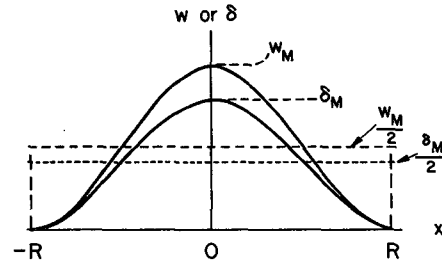


FIG. 19. Horizontal distribution of vertical velocity and of the quantity  $\delta$ , the deviation from its environmental value of a quantity to be mixed, in the cases of sinusoidal (solid) and top-hat (dashed) profiles.

in the sinusoidal case:

$$\begin{aligned} I_S &\equiv \int_0^R \left. \frac{\partial q}{\partial t} \right|_S dx = \int_0^R \delta \frac{1}{M} \frac{\Delta M}{\Delta t} dx = \int_0^R \delta c_M \left| \frac{\partial w}{\partial x} \right| dx \\ &= -c_M \frac{\delta_M}{2} \frac{w_M}{2} \frac{\pi}{R} \int_0^R \left[ 1 + \sin \pi \left( \frac{x}{R} + \frac{1}{2} \right) \right] \\ &\quad \times \cos \pi \left( \frac{x}{R} + \frac{1}{2} \right) dx. \end{aligned}$$

Evaluation of this integral yields

$$I_S = \frac{c_M \delta_M w_M}{2}$$

If one equates the integrated effect of mixing in the two cases, i.e.,

$$I_{\text{TH}} = I_S = \frac{\delta_M w_M}{2} = \frac{c_M w_M \delta_M}{2},$$

then

$$c_M = \alpha.$$

If the values of  $w$  and  $\delta$  in the top-hat profile case are taken to be  $w_M$  and  $\delta_M$ , respectively, rather than  $w_M/2$  and  $\delta_M/2$  (the average values of  $w$  and  $\delta$  in the sinusoidal case), then the result obtained is

$$c_M = 4\alpha.$$

There may be some argument for each of these results so that if the value  $\alpha = 0.1$  is accepted here, the value of  $c_M$  might reasonably be in the range 0.1–0.4. There is some additional reason to expect a certain amount of tolerance in the choice of a value for  $c_M$ , in that the horizontal variation in the vertical velocity in nature need not have a perfectly sinusoidal form. The value used in this study for  $c_M$  is 0.3.

It should be noted here that in nature it is probably true that mixing with the environment occurs along the cloud edges whose properties are then changed, and mixing subsequently occurs between the edges and portions of the cloud nearer the core. The cloud core is

probably affected eventually by this mixing process but to a lesser extent than the edges. Such a detailed process cannot be dealt with explicitly here; the treatment used here is a parameterization of the mixing process. Thus, the mixing at each point is calculated using values of variables in the remote environment rather than using points, for instance, immediately adjacent (as might be done if the mixing were dealt with more explicitly).

## REFERENCES

- Arakawa, A., 1966: Computational design for long-term numerical integration of the equations of fluid motion: Two dimensional incompressible flow, Part I. *J. Comput. Phys.*, **1**, 119-143.
- Árnason, G., R. S. Greenfield and E. A. Newburg, 1968: A numerical experiment in dry and moist convection including the rain stage. *J. Atmos. Sci.*, **25**, 404-415.
- Asai, T., 1964: Cumulus convection in the atmosphere with vertical wind shear: Numerical experiment. *J. Meteor. Soc. Japan*, **42**, 245-259.
- Bates, F. C., 1961: The Great Plains squall line thunderstorm—A model. Ph.D. thesis, St. Louis University.
- Browning, K. A., and F. H. Ludlam, 1962: Air flow in convective storms. *Quart. J. Roy. Meteor. Soc.*, **88**, 117-135.
- Buneman, O., 1969: A compact non-iterative Poisson solver. S.U.I.P.R. Report, AEC Contract AT(04-3)326 PA 20, Institute for Plasma Research, Stanford University, 10 pp.
- Byers, H. R., and R. R. Braham, 1949: *The Thunderstorm*. Washington, D. C., Govt. Printing Office, 287 pp.
- Danielsen, E. F., R. Bleck and D. A. Morris, 1972: Hail growth by stochastic collection in a cumulus model. *J. Atmos. Sci.*, **29**, 135-155.
- Fankhauser, J. C., 1971: Thunderstorm-environment interaction determined from aircraft and radar observations. *Mon. Wea. Rev.*, **99**, 171-192.
- Hane, C. E., 1970: Squall line maintenance: Preliminary numerical investigations. Rept. 70-6, Grant E 22-15-70(G), Dept. of Meteorology, Florida State University, 13 pp.
- , 1972: Squall line structure and maintenance: Numerical experimentation. Ph.D. dissertation, Florida State University.
- Kessler, E., E. Newburg, P. Feteris and G. Wickham, 1961-64: Relationships between tropical precipitation and kinematic cloud models. Repts. 1-5, Contract DA36-039 SC 89099, Travelers Research Center.
- Leith, C. E., 1968: Two dimensional eddy viscosity coefficients. *Proc. WMO/IUGG Symp. Numerical Weather Prediction*, Tokyo, Japan, I-41 to I-44.
- Ludlam, F. H., 1961: The hailstorm. *Weather*, **16**, 152-162.
- Malkus, J. S., and G. Witt, 1959: The evolution of a convective element: A numerical calculation. *The Atmosphere and the Sea in Motion*, B. Bolin, Ed., New York, Rockefeller Institute Press, 425-439.
- Marshall, J. S., and W. McK. Palmer, 1948: The distribution of raindrops with size. *J. Meteor.*, **5**, 165-166.
- Murray, F. W., 1970: Numerical models of a tropical cumulus cloud with bilateral and axial symmetry. *Mon. Wea. Rev.*, **98**, 14-28.
- , and C. E. Anderson, 1965: Numerical simulation of the evolution of cumulus towers. Rept. SU-49230, Douglas Aircraft Company, Inc., Santa Monica, Calif., 97 pp.
- Newton, C. W., 1950: Structure and mechanism of the prefrontal squall line. *J. Meteor.*, **7**, 210-222.
- , 1963: Dynamics of severe convective storms. *Meteor. Monog.*, **5**, No. 27, 33-58.
- Normand, Sir Charles, 1946: Energy in the atmosphere. *Quart. J. Roy. Meteor. Soc.*, **72**, 145-167.
- O'Brien, J. J., 1971: A note on nonlinear eddy viscosity for two-dimensional numerical models. Unpubl. manuscript. Available from Dept. of Meteorology, Florida State University.
- Ogura, Y., 1963: The evolution of a moist convective element in a shallow, conditionally unstable atmosphere: A numerical calculation. *J. Atmos. Sci.*, **20**, 407-424.
- , and J. G. Charney, 1962: A numerical model of thermal convection in the atmosphere. *Proc. Intern. Symp. Numerical Weather Prediction*, Tokyo, Japan, 431-451.
- , and T. Takahashi, 1971: Numerical simulation of the life cycle of a thunderstorm cell. *Mon. Wea. Rev.*, **99**, 895-911.
- Orville, H. D., and J. Y. Liu, 1969: Numerical modeling of precipitation and cloud shadow effects on mountain-induced cumuli. *J. Atmos. Sci.*, **26**, 1283-1298.
- Sasaki, Y., 1959: A numerical experiment for squall line formation. *J. Meteor.*, **16**, 347-353.
- Schlesinger, R. E., 1972: A numerical model of deep moist convection: The influence of ambient conditions and internal physical mechanisms. Studies of the Atmosphere Using Aerospace Probing, Annual Report-1971: Vol. 1, Grant E-230-68-(G), The University of Wisconsin.
- Shapiro, M. A., and J. J. O'Brien, 1970: Boundary conditions for fine-mesh limited-area forecast. *J. Appl. Meteor.*, **9**, 345-349.
- Simpson, J., and V. Wiggert, 1969: Models of precipitating cumulo-fine-mesh limited-area forecasts. *J. Appl. Meteor.*, **9**, 345-349.
- Squires, P., and J. S. Turner, 1962: An entraining jet model for cumulonimbus updraughts. *Tellus*, **14**, 422-434.
- Srivastava, R. C., 1967: A study of the effect of precipitation on cumulus dynamics. *J. Atmos. Sci.*, **24**, 36-45.
- Takeda, T., 1971: Numerical simulation of a precipitating convective cloud: The formation of a "long-lasting" cloud. *J. Atmos. Sci.*, **28**, 350-376.
- Weinstein, A. I., 1970: A numerical model of cumulus dynamics and microphysics. *J. Atmos. Sci.*, **27**, 246-255.